Relationships between spectroscopic properties of high-altitude organic aerosols and Sun photometry from ground-based remote sensing

Natalie Mladenov,[1,2] Isabel Reche,[1] Francisco J. Olmo,[3,4] Hassan Lyamani,[3,4] and Lucas Alados-Arboledas[3,4]

Received 28 February 2009; revised 11 July 2009; accepted 29 September 2009; published 6 February 2010.

[1] Organic aerosols are important light-absorbing compounds in the atmosphere that influence climate by filtering solar radiation and interact with the biosphere via deposition to aquatic and terrestrial ecosystems. There is a limited understanding of their chemical properties and even less is known about the relationships between fluorescent properties and widely used optical properties of aerosols in the vertical air column, such as aerosol optical depth ($\delta_{A\lambda}$), aerosol size distribution, and single scattering albedo ($\omega_{0A\lambda}$). In this study, we examined relationships between spectroscopic (fluorescence and absorbance) properties of the water-soluble organic compounds (WSOC) in aerosol deposition and ground-based remote sensing measurements of aerosols in the atmospheric column. With both techniques, we found important differences between Saharan- and marine-dominated organic aerosols. Saharan-dominated WSOC had more intense fluorescence and higher content of reduced quinone-like fluorescent components than marine-dominated WSOC, and amino acid-like fluorescence was substantial in both types of deposition. Both particulate matter loading and molar absorption in the UV range were significantly related to iron content and may reflect a contribution from iron to light absorption. Saharan-dominated aerosols generally had higher $\delta_{A\lambda}$ and volume concentration of coarse mode particles (>0.5 μm; V_{c2}) than marine-dominated aerosols. Using fluorescence spectroscopy and PARAFAC modeling, we found that reduced quinone-like compounds were significantly and positively related to $\delta_{A\lambda}$ and V_{c2}. The relationships that emerged from this study provide a basis for relating WSOC and columnar measurements in the future.

Citation: Mladenov, N., I. Reche, F. J. Olmo, H. Lyamani, and L. Alados-Arboledas (2010), Relationships between spectroscopic properties of high-altitude organic aerosols and Sun photometry from ground-based remote sensing, *J. Geophys. Res.*, *115*, G00F11, doi:10.1029/2009JG000991.

1. Introduction

[2] Aerosols have an important role in modulating climate and the radiative budget of the atmosphere by scattering and absorbing light and acting as cloud condensation nuclei [*Jacobson et al.*, 2000, and references therein]. A significant portion of high-altitude (>3000 m) aerosols exists as organic matter (OM), representing on average 40% of total particulate matter in fine aerosols ($PM_{2.5}$) [*Krivácsy et al.*, 2001]. Organic aerosols originate from such sources as plant material, bacteria, viruses, fungal spores, primary production over the oceans, biomass and fossil fuel burning, and secondary gas-to-particle conversions [*Jacobson et al.*, 2000]. Some of this material is soluble in water because of its source (e.g., sulfate- and nitrate-containing organic compounds, dicarboxylic acids, polyols, amino acids, and other multifunctional compounds in aerosols) or its interaction with other compounds in the atmosphere (e.g., neutralization of atmospheric acids by alkaline substances in the atmosphere increases solubility) [*Saxena and Hildemann*, 1995]. Therefore, water-soluble organic compounds (WSOC) represent another important fraction of aerosol deposition that is of great consequence for aquatic ecosystems via its role as an energy source for microbes and as a mechanism for attenuating light in the water column [*Mladenov et al.*, 2008; *Reche et al.*, 2009]. WSOC is even present in Saharan dust deposition in amounts that are large enough to replenish the supply of dissolved organic matter (DOM) in alpine lakes located in rocky catchments [*Mladenov et al.*, 2009a].

[3] WSOC optical properties offer important information about the chemical character of aerosol deposition and potentially about the role of aerosols as light scattering

[1]Departamento de Ecología, Universidad de Granada, Granada, Spain.
[2]Institute of Arctic and Alpine Research, University of Colorado at Boulder, Boulder, Colorado, USA.
[3]Centro Andaluz de Medio Ambiente, Granada, Spain.
[4]Departamento de Física Aplicada, Universidad de Granada, Granada, Spain.

0148-0227/10/2009JG000991$09.00

and light absorbing particles. The water-soluble fraction of wet deposition has been analyzed with UV-visible (UV-vis) and fluorescence spectroscopy [*Kieber et al.*, 2006, 2007; *Muller et al.*, 2008], but its presence in dry deposition has received much less attention [*Mladenov et al.*, 2009a] even though it represents the dominant form of deposition in many arid zones, such as the southwest Mediterranean region [*Morales-Baquero et al.*, 2006]. Dry deposition from Saharan dust events is substantial in southern Spain and other Mediterranean countries, and Saharan dust transport has been particularly accentuated in recent decades [*Prospero and Lamb*, 2003].

[4] UV-visible absorption provides important information about the presence of chromophoric compounds [*Morris et al.*, 1995; *Laurion et al.*, 2000; *Andreae and Gelencser*, 2006; *Sun et al.*, 2007] and aromatic structures [*Weishaar et al.*, 2003] in DOM and WSOC. Fulvic and humic-like substances (HULIS) fall within a larger category of light absorbing organic matter, also known as brown carbon (C_{brown}), that is not black (BC) or elemental carbon (EC). C_{brown} absorbs most strongly in the UV range [*Andreae and Gelencser*, 2006] but also has substantial absorption in the visible range, where nearly 40% of the solar energy is found [*Sun et al.*, 2007].

[5] In addition to light absorption by organic compounds in aerosols, the contribution of iron (Fe) oxides to aerosol optical properties must also be considered because of the high content of Fe in dust [*Jickells et al.*, 2005]. In particular, Fe oxides in mineral dust influence light absorption and scattering in the UV and visible range [*Alfaro et al.*, 2004; *Linke et al.*, 2006]. Ferric iron is the form that most strongly affects UV absorbance, with absorbance peaks between 200 and 250 nm and 290 and 320 nm [*Steiner and Lazaroff*, 1974].

[6] Whereas absorption describes the UV and visible light absorbing properties of water-soluble aerosols, fluorescence spectroscopy can further discriminate the light-absorbing compounds that might be present, allowing for the identification of amino acid-like and quinone-like compounds that have the ability to fluoresce. Recent advances in fluorescence spectroscopy with parallel factor analysis (PARAFAC) modeling can quantify the distribution of fluorescent compounds [*Stedmon et al.*, 2003]. *Mladenov et al.* [2009a] found that Saharan dust events contained water-soluble organic aerosols in which quinone-like fluorescence was dominant and present in the same spectral regions where HULIS has been shown to fluoresce in other studies [*Duarte et al.*, 2004]. DOM fluorescence is influenced by its conformation and chemical structure. For example, HULIS fluorescence is representative of higher molecular weight, macromolecular compounds [*Muller et al.*, 2008] potentially associated with larger aerosol particle sizes.

[7] Ground-based aerosol remote sensing provides information about the optical and physical properties of aerosols in a vertical air column and these data represent critical inputs to aerosol radiative forcing models. The basic columnar optical and physical parameters obtained from ground-based aerosol remote sensing by Sun photometry and sky radiance are aerosol optical depth($\delta_{A\lambda}$), Angström exponent (α), single scattering albedo ($\omega_{0A\lambda}$), particle radius (r), and volume size distribution (V(r)). $\delta_{A\lambda}$ is a quantitative measure of the extinction of solar radiation by aerosol scattering and absorption, while α is derived from $\delta_{A\lambda}$ measurements and gives an indication of the column integrated aerosol size distribution. $\omega_{0A\lambda}$ represents the ratio of scattering to scattering + absorption, and r and V(r) provide particle size distribution information for coarse and fine mode particles. These aerosol remote sensing data characterize the vertical air column at a higher frequency than passive collection using standard dry and wet deposition samplers and provide immediate information. Yet spectroscopic analyses of dry deposition offer detailed insight into the chemical character of aerosols and, specifically, the presence of light-absorbing compounds, such as brown carbon, HULIS, and Fe. Therefore, the establishment of relationships between both procedures can be useful to inform both the aquatic and atmospheric sciences. On the one hand, such relationships may be extrapolated to long-term global data sets of ground-based aerosol remote sensing, which have higher temporal and spatial resolution. Those data can then make available more information or help fill in the gaps about the organic aerosol properties that may have dominated at a certain time and place. On the other hand, relationships between ground-based aerosol remote sensing and dry deposition chemical properties can be used to inform aerosol modeling studies about organic aerosol chemistry.

[8] In an effort to elicit important and meaningful relationships between aerosol columnar properties and optical properties of high-altitude aerosol deposition, we examined trends between particulate matter (PM) and OM deposition loading, Fe content, WSOC absorption and fluorescence, and the optical properties derived from ground-based remote sensing ($\delta_{A\lambda}$, $\omega_{0A\lambda}$, r, and V(r)). Because ground-based remote sensing by Sun photometry does not perform optimally under cloud cover or during rain events, we removed wet deposition results from our study and focused on dry deposition samples. To our knowledge, this is the first study to examine WSOC fluorescence and columnar aerosol relationships.

2. Methods

2.1. Sample Collection

[9] Samples of dry deposition were collected every 14 days during the summer of 2007 and every 7 days during the summer of 2008 using a MTX1 ARS 1010 automatic deposition sampler (that allows for separate collection of wet deposition), located at 2896 m above sea level (asl) (37°03′N, 3°23′W) at the Sierra Nevada Observatory (OSN) station at Loma de Dilar in the Sierra Nevada mountain range (Spain). At the high elevation of the OSN station, the organic aerosols originate mainly from Saharan and marine sources rather than from combustion or biomass burning. The columnar aerosol data were retrieved in Granada (Spain), a nearby site with some known urban influence, but with a consistent summer pattern of discernable Saharan dust events recorded in columnar aerosol properties [*Lyamani et al.*, 2006a, 2006b; *Alados-Arboledas et al.*, 2008]. For comparison with Sun photometer data, this study analyzed results of dry deposition collection only. More details on atmospheric deposition collection can be found elsewhere [*Morales-Baquero et al.*, 2006].

2.2. Particulate Matter and WSOC Analyses

[10] PM loadings (mg m^{-2} d^{-1}) were obtained by rinsing the dry deposition receptacle for 10–15 min with 1 L of high-quality Milli-Q water. Approximately 500 mL of the suspension was filtered through precombusted (500°C for 4 h) and preweighed Whatman GF/F filters with 0.7 μm nominal pore size. The filters containing PM were dried at 50°C for >24 h and reweighed to determine the PM mass. The filters were then combusted at 500°C for 4 h and reweighed to determine the water-insoluble organic compound (WINSOC) mass. The filtrates, referred to as WSOC, were stored in precombusted amber glass bottles at approximately 4°C in the dark until analysis. WSOC samples for spectroscopic analyses were stored unacidified, and samples for dissolved organic carbon (DOC) concentration measurements were acidified to a pH of 2 with concentrated HCl or H_3PO_4. Loadings (mg m^{-2} d^{-1}) were calculated by normalizing PM and WINSOC mass or DOC concentration to the volume of Milli-Q water used, area of the bucket, and length of collection period (days). Total organic carbon (TOC) was computed as the WINSOC + WSOC.

[11] DOC concentration was measured as nonpurgable organic carbon on filtered-acidified dry deposition WSOC solutions within one month of collection using a Shimadzu TOC-V CSH equipped with a high-sensitivity catalyst. The DOC concentration of WSOC extracted from dry deposition is referred to here as WSOC concentration [WSOC]. [WSOC] was measured in duplicate for each sample and replicates were included within runs and over time, with standard deviations within 5%, on average. UV-vis absorbance scans were measured in duplicate within a month of collection at a range of 250–900 nm in 10 cm path length quartz cuvettes using a Perkin Elmer Lambda 40 spectrophotometer connected to a computer equipped with UV-Winlab software. The absorbance value at 690 nm was used to correct UV absorbance values for scattering [*Laurion et al.*, 2000]. Absorbance at 250 nm, 280 nm, 320 nm, 365 nm, and 440 nm wavelengths were expressed as Naperian absorption coefficients (a_{250}, a_{280}, a_{320}, a_{365}, and a_{440}) and were calculated by multiplying the absorbance values by 2.303 and dividing by the optical path length in m. The molar absorption coefficient (ε) (m^2 mol^{-1}) was calculated by dividing the absorption coefficient at each wavelength by the DOC concentration in mmol L^{-1}. The molar absorption coefficient at wavelengths between 250 and 280 nm, where aromatic moieties absorb most strongly, is often used to evaluate the contributions of vascular plant sources and organic soil to the DOM pool [*Chin et al.*, 1994; *Weishaar et al.*, 2003]. Absorption between 250 and 280 nm also indicates the presence of the aromatic amino acids, tryptophan, tyrosine, and phenylalanine, which absorb most strongly at these lower wavelengths [*Ross*, 1934]. Values are also reported for 320 nm, one of the wavelengths commonly used to refer to color and UV transparency in the water column [*Morris et al.*, 1995], for 365 nm, which is used to calculate the spectral ratio of a_{250}: a_{365}., and for 440 nm, a wavelength in the photosynthetically active radiation (PAR) wave band.

[12] Fluorescence spectroscopy can provide valuable insights into the sources of DOM in aquatic and aerosol deposition samples and various treatments of fluorescence data have been published, including generation of excitation emission matrices (EEMs) [*Coble*, 1996; *Decesari et al.*, 2001], determination of the fluorescence index (FI) [*McKnight et al.*, 2001], evaluation of fluorescent peak positions [*Coble*, 1996], and PARAFAC modeling [*Stedmon et al.*, 2003; *Cory and McKnight*, 2005], although the application of PARAFAC to organic aerosols is just beginning [*Mladenov et al.*, 2009a]. EEMs are a three-dimensional representation of fluorescence intensities scanned over a range of excitation:emission (Ex/Em) wavelengths. Prominent humic peaks have been found in EEMs, one stimulated by UV excitation (at Ex/Em 240–260/380–460 nm) and another stimulated by visible excitation (at Ex/Em 320–350/420–480 nm). Other peak areas are attributed to tyrosine and tryptophan amino acid fluorescence at 275/310 nm and 275/340 nm [*Coble*, 1996]. EEMs were measured using JY-Horiba Spex Fluoromax-3 (for WSOC collected in 2007) and JY-Horiba Spex Fluoromax-4 (for WSOC collected in 2008) spectrophotometers and were scanned using an integration time of 0.25 s over an excitation range of 240–450 nm at 10 nm increments (and later interpolated to 5 nm increments) and an emission range of 350–550 nm at 2 nm increments. Because of the low DOC concentration and absorbance of deposition samples, no inner-filter effect correction was applied. To correct for lamp spectral properties and to be able to compare results between the Fluoromax-3 and Fluoromax-4 instruments and with fluorescence reported in other studies, spectra were collected in signal-to-reference (S:R) mode and instrument-specific excitation and emissions corrections were applied. Corrections and generation of EEMs were performed using MATLAB. Then all samples were normalized to the Raman area to account for lamp decay over time and Milli-Q water blanks were subtracted to remove Raman scattering. The spectra of quinine sulfate measured on Fluoromax-3 and Fluoromax-4 instruments matched the (NIST) reference spectrum of quinine sulfate [*Velapoldi and Mielenz*, 1981], measured at excitation 350 nm, with a peak at 450 nm emission.

[13] To identify the multiple fluorescent components that comprise the EEMs of dry deposition WSOC, EEMs were fit to a 13-component PARAFAC model [*Cory and McKnight*, 2005] that contains a diverse range of samples but does not include any samples derived from WSOC. While this approach is useful for comparing results with other studies that use the same model, a PARAFAC model created exclusively for aerosol samples would provide greater interpretive power. For the current approach, PARAFAC distributions were not used if intensities in the residual model, generated by subtracting the PARAFAC modeled EEM from the measured EEM, were >10% of measured intensities. Prior to model fitting, Rayleigh scatter bands (first order at each wavelength pair where Ex = Em ± band pass; second order at each wavelength pair where Em = 2 * Ex ± (2 * band pass)) were excised. Of the thirteen components identified by the Cory and McKnight PARAFAC model, there are three components with fluorescence maxima positions similar to oxidized quinones (Q) (C2, C11, and C12); four similar to reduced semiquinones (SQ) and a hydroquinone (HQ) (C5, C7, C9, and C4, respectively); and two amino acid-like components similar in fluorescence intensity to that of trypophan and tyrosine (C8 and C13, respectively) [*Cory and McKnight*, 2005]. Here we report the fluorescence index (FI) as defined by

Cory and McKnight [2005], the total fluorescence, and the fluorescence loading of each component in Raman units (RU) [*Stedmon et al.*, 2003] and, to account for concentration effects, we report the fluorescence on a molar basis for each component (*f*C1, *f*C2, . . .*f*C13) by dividing the fluorescence loading by the DOC concentration of the WSOC solution [*Mladenov et al.*, 2009a]. Changes in FI > 0.05 have been shown to indicate a change in DOM source [*Hood et al.*, 2003; *Mladenov et al.*, 2005]. We also report the relative amount (%) of total amino acid-like (AA), reduced quinone-like, and oxidized quinone-like components.

[14] The mineralogical composition of dust aerosols, mostly iron oxides, can affect their optical properties [*Linke et al.*, 2006]. Therefore, we measured the total iron content in the collected aerosols following standard protocols [*American Public Health Association* (*APHA*), 1992]. Briefly, 50 ml samples from the collectors were acidified with nitric acid, heated at 80°C for 24 h, acidified with hydrochloric acid, and heated again for 24 h. The sample volume was adjusted to the initial volume and total iron was measured by flame atomic absorption spectrometry.

2.3. Ground-Based Remote Sensing Parameters

[15] In order to obtain an atmospheric columnar characterization of the aerosol load we used a Cimel CE-318 Sun photometer, which is the standard Sun/sky photometer used in the AERONET network [*Holben et al.*, 1998]. The Sun photometer was mounted on the roof of the Andalucian Environmental Center in Granada (CEAMA), Spain (referred to as the Granada station). Instrument-specific settings are described in detail by *Holben et al.* [1998] and *Lyamani et al.* [2006a, 2006b]. In brief, the automatic tracking Sun and sky scanning radiometers make solar direct irradiance measurements with a 1.2° full field of view at 340, 380, 440, 670, 870, 940, and 1020 nm, and sky radiance almucantar measurements at 440, 670, 870 and 1020 nm (nominal wavelengths). $\delta_{A\lambda}$ was computed at 440, 670, 870 and 1020 nm (nominal wavelengths). Calibration of the instrument was performed at 2200 m asl in the Sierra Nevada at least twice a year using the Langley plot technique for direct Sun measurements and an integrating sphere for radiance measurements [*Alcántara et al.*, 2004; *Alados-Arboledas et al.*, 2008].

[16] For the retrieval of aerosol optical properties, we first removed cloud-contaminated measurements by using the cloud screening method by *Smirnov et al.* [2000]. Even if data passed the threshold screening test, we only used data within three standard deviations from the mean in order to further reduce uncertainties induced by cloud interference.

[17] The aerosol optical depth, $\delta_{A\lambda}$ (dimensionless), is derived from the total optical depth, δ_{λ}, obtained from direct Sun photometer measurements data using the appropriate calibration constant and subtracting the Rayleigh optical depth, $\delta_{R\lambda}$, as well as the O_3 and NO_2 absorption optical depths, $\delta_{3\lambda}$ and $\delta_{2\lambda}$ [*Alados-Arboledas et al.*, 2003; *Lyamani et al.*, 2005].

[18] The Angström wavelength exponent, α (dimensionless), which is a measure of the wavelength λ dependence of aerosol optical depth, is computed from aerosol optical depth data assuming the model proposed by Angström, described by *Lyamani et al.* [2006b]. In this way, the Angström exponent characterizes the spectral features of aerosol particles and is related to the size of particles. Large values of α indicate the prevalence of fine particles from urban-industrial and biomass burning sources, while low values of α are related with the presence of coarse particles such as desert dust and marine aerosols [*Lyamani et al.*, 2006b].

[19] The sky radiance almucantar measurements at 440, 670, 870, and 1020 nm in conjunction with solar direct irradiance and aerosol optical depth measurements at these same wavelengths, were utilized to retrieve the single scattering albedo, $\omega_{0A\lambda}$, the volume concentrations of fine and coarse mode particles (V_{c1} and V_{c2}, respectively), and the effective radius based on the method of *Nakajima et al.* [1996] using the nonspherical approach proposed by *Olmo et al.* [2006, 2008]. The effective radius is defined as the area weighted mean radius of the aerosol particles. The aerosol size distribution and $\omega_{0A\lambda}$ were derived by iteration, minimizing the residuals between measured and calculated radiances. V_{c1}, V_{c2}, and effective radius were computed by formulating the equations described by *Dubovik et al.* [2002] to give the parameters of a bimodal lognormal size distribution. In our case, this resulted in two modes corresponding to submicron ($r < 0.5$ μm) and micrometric ($r \geq 0.5$ μm) particles, from which V_{c1} and V_{c2}, respectively, were derived.

[20] The $\omega_{0A\lambda}$ (dimensionless) is a key parameter for the estimation of the direct radiative impact of aerosols. It depends on the relative source strengths of the various aerosol substances and aging during transport.

2.4. Data Analyses

[21] For comparison with the weekly (2008) and fortnightly (2007) dry deposition data, all ground-based remote sensing data ($\delta_{A\lambda}$, α, $\omega_{0A\lambda}$, effective radius, and V(r)) were converted from hourly averages to weekly or fortnightly measurements by weighted averaging, whereby data were first averaged on a daily basis and then on a 7 day or 14 day basis. To test for significant relationships between parameters, linear and multiple regressions were performed using Statistica software. Significant relationships are reported for $p < 0.05$ and $p < 0.01$. We further examined relationships for periods with PM loadings >50 mg m^{-2} d^{-1}, which corresponded roughly to the periods that had Saharan dust events.

[22] We examined the source of air masses over the Sierra Nevada, Spain, by computing daily backward trajectories (http://www.arl.noaa.gov/ready.html) using the HYSPLIT model [*Draxler and Rolph*, 2003] with archived data from the Global Data Assimilation System (GDAS) data set with 120 h run time. These backward trajectories were consulted for each day of each sampling period to verify the sources of air masses, with North African (referred to as Saharan) and Atlantic or Mediterranean (referred to as marine) emerging as the most dominant. Representative trajectories are shown for Saharan- and marine-dominated periods (Figure 1). In addition, we consulted daily Light Detection and Ranging (LIDAR) vertical profiles measured at the Granada station from 27 July to 10 October 2007 and from 24 July to 15 August 2008 [*Guerrero-Rascado et al.*, 2008]

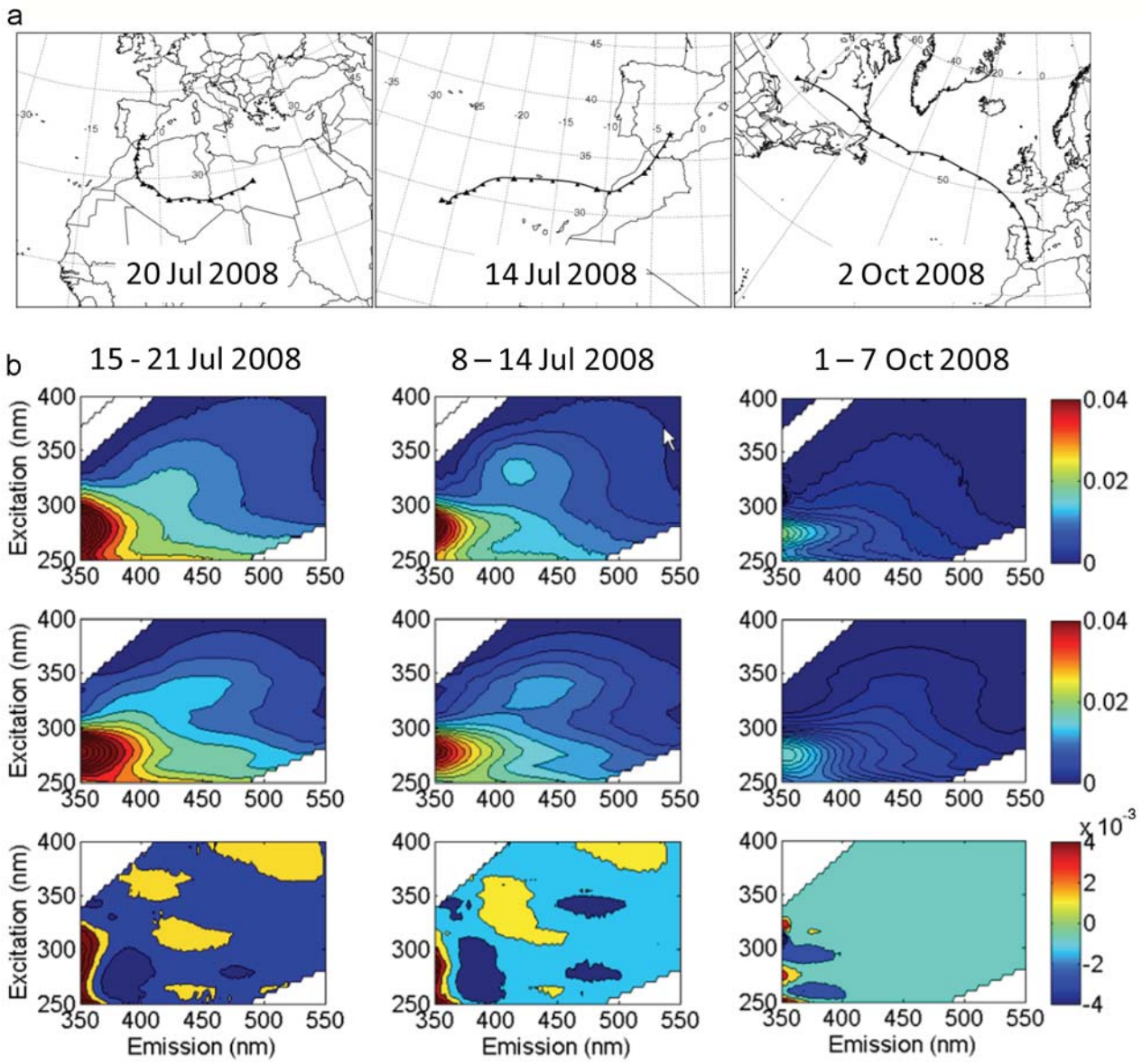

Figure 1. (a) Representative 5 day backward trajectories at 3000 m asl corresponding to each period. (b) Excitation-emission spectra for representative Saharan-dominated and marine-dominated collection periods; (left) 7 out of 7 Saharan days, (middle) 4 out of 7 Saharan days, and (right) 5 out of 7 marine days. (top) Measured EEMs, (middle) PARAFAC modeled EEMs, and (bottom) residual EEMs are shown with intensities measured in Raman units.

to determine the elevation of the Planetary Boundary Layer and the presence of atmospheric aerosols at the level of the high-elevation mountain site. Temporal evolutions of LIDAR signals acquired from the Granada station were multiplied by the square of the distance to correct for the effect of LASER beam divergence (range-corrected signals) [*Guerrero-Rascado et al.*, 2008]. The short horizontal separation between the Granada and OSN stations allows us to consider both stations as located in approximately the same vertical column. This fact is especially important when considering relationships between the high mountain samples and the vertical profiles of atmospheric aerosol retrieved by the LIDAR system operated at the Granada station [*Alados-Arboledas et al.*, 2007]. The Raman LIDAR system configuration is described by *Guerrero-Rascado et al.* [2008].

3. Results

3.1. Particulate and Organic Matter Deposition

[23] Aerosol deposition data were separated into two main groups based on the dominant origin of aerosols (Saharan and marine) (Table 1), and representative backward trajectories are shown for each type of sampling period (Figure 1). The PM loading values ranged from 7 to 138 mg m^{-2} d^{-1}, and most collection periods with a high PM loading corresponded to Saharan-derived aerosol deposition

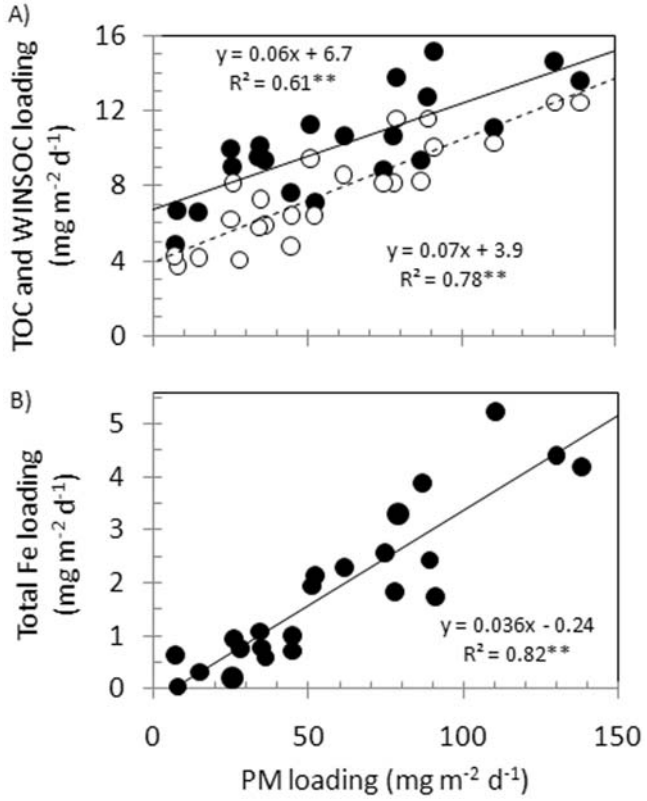

Figure 2. Relationships between (a) the loadings of total organic carbon (TOC, solid circles) and water-insoluble organic compounds (WINSOC, open circles) and the particulate matter (PM) and (b) the loadings of total iron (Fe) and PM. Regression line equations, R^2 values, and significance (** $p < 0.01$) are shown.

(Table 1). Five collection periods, almost entirely dominated by marine air masses, had substantially lower mean PM, TOC, and WSOC deposition loadings than Saharan-dominated collection periods (Table 1). For all collection periods, TOC loading was on average 26% of the PM loading, and the soluble portion (WSOC) was approximately 16% of the TOC loading and 4% of the PM loading. As PM loading increased, the WINSOC portion increased significantly ($p < 0.01$; Figure 2a), while no relationship was found with WSOC loading. Iron content in deposition samples ranged from 0.03 to 5.2 mg m^{-2} d^{-1}, with higher values during Saharan dominated events (Table 1). There was a significant relationship between total iron loading and PM loading ($R^2 = 0.82$; $p < 0.01$, $n = 23$; Figure 2b).

[24] With greater WSOC loading, absorbance and fluorescence increased significantly (Figures 3a and 3b). The 2007 deposition, collected over a 14 day period, had considerably higher a_{320}, f_{total}, and cumulative WSOC loading than the 2008 deposition, collected over a 7 day period (Figure 3b) and this concentration effect prompted the use of molar absorption and molar fluorescence in this study. Molar absorption coefficients at 250 nm, 280 nm, 320 nm and 365 nm ranged from 0 to 44 m^2 $mmol^{-1}$, 0 to 62 m^2 $mmol^{-1}$, 0 to 13 m^2 $mmol^{-1}$, 0 to 8.5 m^2 $mmol^{-1}$, respectively. Saharan-dominated periods consistently had higher means and ranges of a and ε at each wavelength than marine-dominated periods (Figure 3a and Table 1). Only 11 out of 24 sampling periods had measurable absorbance in the visible range (>400 nm). The total Fe concentration of dry deposition samples was significantly related to the molar absorption coefficient, but with low explained variance (the highest R^2 was 0.32 for ε_{320} and ε_{365}; $p < 0.05$; $n = 21$).

[25] The fluorescent properties of Saharan-derived WSOC generally reflected more terrestrial OM sources (lower FI) and a greater content of reduced fluorescent components (higher RI) than marine-derived WSOC (Table 1). EEMs of marine-dominated deposition were dominated mainly by amino acid-like fluorescence (Ex/Em 250–280/350–365) (Figure 1). Saharan-dominated deposition had intense amino acid-like fluorescence as well as fluorescent shoulders centered on Ex/Em 240–250/425 and 320–340/425–450 (Figure 1). For most cases, the fit of measured EEMs to the PARAFAC model generated residual EEMs with fluorescence intensities <10% of the measured EEM (Figure 1). Model results from three collection periods (24–30 June, 29–4 August, and 23–29 September 2008) were not used because they did not meet this criterion. For all other periods, PARAFAC distributions indicated that total quinone-like fluorescence was higher in Saharan than marine-dominated deposition in terms of both loading and molar fluorescence. Reduced quinone-like components, in particular C4, were generally more prevalent in EEMs of Saharan aerosols whereas amino acid-like components, namely tryptophan-like (*f*C8), were higher in the EEMs of marine aerosols (Table 1). Only *f*C3 and *f*C7, which together represent less than 7% of the total fluorescence, were significantly related to the total Fe concentration, but with low explained variance ($R^2 = 0.29$ and 0.32, respectively; $p < 0.05$; $n = 19$). The influence of Fe-DOM complexation on the EEMs of WSOC was not evaluated.

3.2. Ground-Based Remote Sensing

[26] During the summers of 2007 and 2008, $\delta_{A\lambda}$ ranged from 0.06 to 0.27 and $\omega_{0A\lambda}$ ranged from 0.82 to 0.98. For periods with Saharan events, both $\delta_{A\lambda}$ and $\omega_{0A\lambda}$ were higher, ranging from 0.11 to 0.28 (at 670 nm) and from 0.81 to 0.92 (at 670 nm), respectively (Table 2). α values were generally higher for marine-dominated than for Saharan-dominated periods (Table 2).

[27] V_{c1} was similar for Saharan- and marine-dominated periods, while V_{c2} values were higher for Saharan-dominated periods, ranging from 0.09 to 0.31 μm^3 μm^{-2} (Table 2).

[28] The $\delta_{A\lambda}$ (670) was related positively and significantly ($R^2 = 0.53$; $p < 0.01$; $n = 24$) to volume concentration of the coarse mode, V_{c2}, (Figure 4). To verify that the 7 day and 14 day averaging did not influence these results, we also examined this relationship for a subset of daily averages and found that it was significant ($R^2 = 0.90$; $p < 0.01$; $n = 96$) and similar in slope to that reported in Figure 4.

[29] Temporal evolutions of LIDAR signals from a date with marine aerosol sources, representative of periods with low PM loading, and from a date with a Saharan dust intrusion, representative of periods with high PM loading, both show large signals representative of high concentration of aerosols <2000 m asl (Figures 5a and 5b). During the Saharan event, a high concentration of dust particles was present above 3000 m asl, but during the marine event there was an absence of aerosol particles at this level.

Table 1. Representative and Mean Values for Particulate Matter, Total Organic Carbon, Water-Insoluble Organic Carbon, and Water-Soluble Organic Compound Loading, Absorption, Iron Content, Fluorescence Properties, and PARAFAC Component Distribution, as Loadings and Molar Fluorescence *f*C, for Each Collection Period[a]

		Saharan-Dominated (n = 12)		Marine-Dominated (n = 5)	
Properties[b]	Units	15–21 July 2008	Mean	1–6 October 2008	Mean
PM loading	mg m^{-2} d^{-1}	79	71 (26–138)	7	36 (7–87)
WINSOC loading	mg m^{-2} d^{-1}	12	9 (4–12)	4	6 (4–8)
WSOC loading	mg m^{-2} d^{-1}	2.2	2.4 (0.8–5.0)	0.6	1.8 (0.6–3.8)
TOC loading	mg m^{-2} d^{-1}	14.2	11 (8–15)	4.6	8 (5–10)
Total Fe loading	mg m^{-2} d^{-1}	3.29	2.22 (0.94–5.23)	0.63	1.37 (0.03–3.88)
ε_{250}	m^2 $mmol^{-1}$	15.7	22.3 (6.3–43.5)	0.0	13.4 (0–27.0)
ε_{280}	m^2 $mmol^{-1}$	12.0	21.3 (4.7–62.4)	0.0	8.8 (0–19.5)
ε_{320}	m^2 $mmol^{-1}$	5.2	4.6 (1.6–12.9)	0.0	2.5 (0–5.3)
ε_{365}	m^2 $mmol^{-1}$	2.9	2.4 (0.7–8.5)	0.0	1.1 (0–3.2)
ε_{440}	m^2 $mmol^{-1}$	1.2	1.3 (0.1–4.6)	0.0	0.4 (0–1.3)
FI	-	1.23	1.41 (1.23–1.65)	1.42	1.45 (1.39–1.51)
RI	-	0.37	0.42 (0.33–0.49)	0.27	0.34 (0.27–0.46)

		15–21 July 2008		Mean		1–6 October 2008		Mean	
PARAFAC Component Data	Location of Ex/Em Peaks[c]	Loading[d] (RU)	*f* (RU mM^{-1})	Loading[d] (RU)	*f* (RU mM^{-1})	Loading[d] (RU)	*f* (RU mM^{-1})	Loading[d] (RU)	*f* (RU mM^{-1})
Total fluorescence	-	0.164	1.89	0.132	1.59	0.036	1.61	0.075	1.39
AA fluorescence	-	0.070 (43)	0.81	0.032 (21)	0.58	0.018 (50)	0.79	0.023 (26)	0.86
RQ fluorescence	-	0.025 (15)	0.29	0.032 (26)	0.34	0.004 (11)	0.16	0.014 (20)	0.20
OQ fluorescence	-	0.043 (26)	0.50	0.041 (32)	0.47	0.010 (28)	0.44	0.024 (34)	0.40
C1(unk)	340/450	0.011 (7)	0.13	0.009 (7)	0.12	0.002 (5)	0.08	0.005 (6)	0.09
C2 (Q2)	250/458	0.019 (11)	0.22	0.017 (13)	0.20	0.004 (11)	0.17	0.010 (12)	0.17
C3 (unk)	315/386	0.014 (9)	0.16	0.007 (6)	0.09	0.000 (1)	0.01	0.003 (3)	0.05
C4 (HQ)	250/550	0.019 (12)	0.22	0.021 (15)	0.22	0.003 (7)	0.12	0.010 (12)	0.15
C5 (SQ1)	295/516; 380/516	0.002 (1)	0.02	0.003 (2)	0.03	0.000 (1)	0.01	0.001 (1)	0.01
C6 (unk)	270/430	0.000 (0)	0.00	0.002 (2)	0.03	0.001 (2)	0.03	0.002 (2)	0.02
C7 (SQ2)	270/462; 380/462	0.004 (3)	0.05	0.004 (3)	0.05	0.001 (2)	0.03	0.002 (2)	0.03
C8 (Trp)	270/360	0.031 (19)	0.36	0.016 (12)	0.26	0.011 (31)	0.50	0.012 (19)	0.48
C9 (SQ3)	345/410; 265/410	0.000 (0)	0.00	0.004 (3)	0.04	0.000 (1)	0.01	0.001 (1)	0.01
C10 (unk)	305/426	0.000 (0)	0.00	0.008 (6)	0.10	0.002 (6)	0.10	0.005 (6)	0.06
C11 (Q1)	260/440	0.005 (3)	0.05	0.007 (5))	0.07	0.000 (1)	0.02	0.005 (5)	0.05
C12 (Q3)	250/388	0.019 (12)	0.22	0.017 (13)	0.20	0.005 (15)	0.25	0.010 (13)	0.18
C13 (Tyr)	280/350	0.039 (24)	0.45	0.016 (14)	0.33	0.006 (18)	0.29	0.012 (13)	0.39

[a]Range shown in parentheses.
[b]PM, particulate matter; TOC, total organic carbon; WINSOC, water-insoluble organic carbon; WSOC, water-soluble organic compound; FI, fluorescence index; RI, redox index; AA, amino acid-like (C8 + C13); RQ, reduced quinone-like (C4 + C5 + C7 + C9); OQ, oxidized quinone-like (C2 + C11 + C12); Q, quinone-like; SQ, semiquinone-like; HQ, hydroquinone-like; Trp, tryptophan-like; Tyr, tyrosine-like; unk, unknown association. Molecular association from *Cory and McKnight* [2005].
[c]Only most intense peaks listed for each component [*Cory and McKnight*, 2005].
[d]Loadings are reported per 7 day collection periods. The percent of total fluorescent loading is shown in parentheses.

3.3. Relationships Between Aerosol Deposition and Ground-Based Remote Sensing Data

[30] We found significant relationships between dry deposition loadings, fluorescence of WSOC, and columnar aerosol properties. WINSOC loading and $\omega_{0A\lambda}$ were positive and significantly related ($R^2 = 0.25$; $p < 0.05$; $n = 23$) when all data were considered, but this relationship was not significant when only PM loadings >50 mg m^{-2} d^{-1} were used. Negative and significant relationships ($R^2 = 0.34$; $p < 0.05$; $n = 22$) were obtained for WSOC and $\omega_{0A\lambda}$ at all wavelengths when all data were considered. This relationship also was not significant when only data with PM loadings >50 mg m^{-2} d^{-1} were considered.

[31] The $\delta_{A\lambda}$ values were significantly related (at all wavelengths; only results for 670 nm shown) to the molar fluorescence of the sum of reduced quinone-like components (*f*RQ), ($R^2 = 0.33$; $p < 0.01$; $n = 19$), and particularly with *f*C4 for all sampling periods as well as for periods with PM loadings >50 mg m^{-2} d^{-1} (Figure 6a). We also obtained significant relationships between V_{c2} and *f*RQ ($R^2 = 0.46$; $p < 0.01$; $n = 19$), particularly accentuated for *f*C4 (Figure 6b). Multiple regression analyses did not identify Fe as a significant predictor of variation for $\delta_{A\lambda}$ values or V_{c2} and no significant relationships existed between total Fe content and other columnar aerosol properties.

4. Discussion

4.1. Differences Between Saharan- and Marine-Dominated Aerosols

[32] The higher PM loading observed for Saharan-dominated periods than for marine-dominated periods is consistent with previous findings by *Mladenov et al.* [2009a] and supports other studies [*Morales-Baquero et al.*, 2006; *Pulido-Villena et al.*, 2006; *Mladenov et al.*, 2008] that attribute high dry deposition loadings during summers to Saharan dust events. The mean WSOC fraction of the TOC loading, however, was lower (14%) than other studies that report it between 38% and 77% for rural and high-altitude sites [*Jaffrezo et al.*, 2005, and references therein]. Although

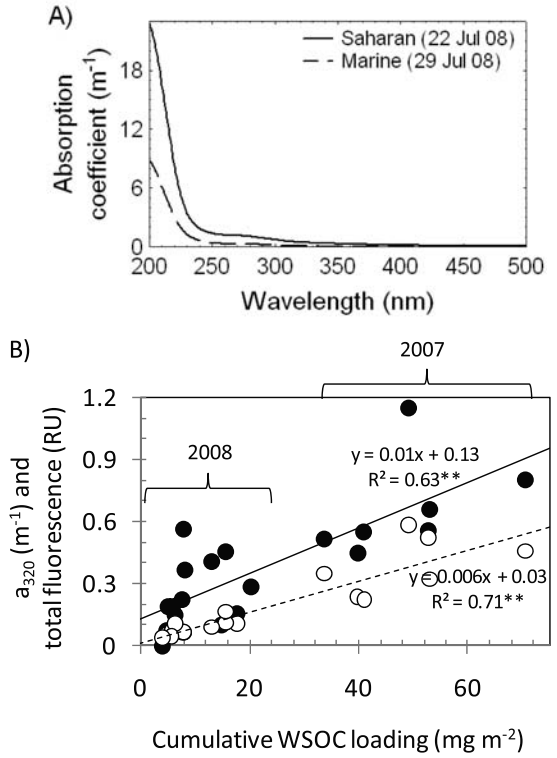

Figure 3. (a) Absorption curves for Saharan (solid line) and marine (dashed line) sampling periods and (b) relationships between absorption at 320 nm (a_{320}) and cumulative water-soluble organic compounds (WSOC) loading (solid circles) and total fluorescence intensity and WSOC (open circles). The data for 2007 (2 week sampling) and 2008 (1 week sampling) are indicated. Regression line equations, R^2 values, and significance (** $p < 0.01$) are shown.

there are methodological differences between these studies (all particle sizes in passive collection versus only particles <10 μm (PM_{10}) in active collection), this difference may suggest that the organic material deposited in the Sierra Nevada is less soluble than organic aerosols at other remote sites. The highly significant relationship between PM loading and total Fe content (Figure 2b) is consistent with previous findings of high Fe content in desert dust aerosols [*Jickells et al.*, 2005].

[33] Our findings of higher absorption and molar absorption of WSOC from Saharan than marine-dominated periods are also consistent with those of *Mladenov et al.* [2009a] showing that Saharan-dominated periods contained more aromatic and chromophoric WSOC than marine-dominated periods. The values for Saharan-dominated periods (from 4.7–62.4 m^2 $mmol^{-1}$ for ε_{280}) are in the range reported by *Duarte et al.* [2004] for WSOC extracted from aerosols in a rural area in Portugal (from 1–2 L g^{-1} cm^{-1} or 28–55 m^2 $mmol^{-1}$ for ε_{280}) and fall in the range of Lake Fryxell fulvic acid and Suwannee River Reference fulvic acid ε_{280} values (0.8 and 2.5 L mg^{-1} m^{-1}, or 22 and 69 m^2 $mmol^{-1}$, respectively [*Mladenov et al.*, 2007]). Marine-dominated ε_{280} values were well below these WSOC and aquatic fulvic acid ranges. Relationships between total Fe content of dry deposition and molar absorption suggest that absorption by Fe could account for some portion of the light absorption. Although we did not measure the Fe content of the water-soluble fraction explicitly, this relationship between total Fe content (particulate + dissolved) and molar absorption of the water-soluble fraction further suggests that the solubility of Fe, which is generally considered to be very low under oxidizing conditions above pH 4, may be enhanced in the presence of organic matter via organic complexation, as has been previously suggested [*Jickells et al.*, 2005].

[34] Also, it has been proposed that thermodynamically stable iron oxides in aerosols may undergo reductive dissolution during long-range transport, triggered by light-induced and thermal dissolution in the presence of reductants or ligands, such as oxalate, in the atmosphere [*Sulzberger and Laubscher*, 1995]. Recently, the electron shuttling ability of humic substances has been implicated in the reductive dissolution of iron oxides in groundwater [*Mladenov et al.*, 2009b]. A similar role for HULIS as an influence on iron solubility in aerosols merits further study.

[35] The higher total fluorescence loading of Saharan-dominated deposition indicates that Saharan air masses deposit higher amounts of fluorescent organic material than

Table 2. Aerosol Columnar Properties for Representative Collection Periods and Mean Values for Each Collection Period[a]

		Saharan (n = 12)		Marine (n = 5)	
Properties[b]	Units	1–14 August	Mean	1–6 October	Mean
Saharan backtrajectories	days	7/7	-	0/7	-
Marine backtrajectories	days	0/7	-	5/7	-
δ_A (440 nm)	-	0.26	0.16 (0.10–0.26)	0.06	0.08 (0.06–0.11)
δ_A (670 nm)	-	0.28	0.17 (0.11–0.28)	0.07	0.09 (0.07–0.12)
δ_A (870 nm)	-	0.30	0.19 (0.11–0.30)	0.09	0.11 (0.09–0.12)
δ_A (1020 nm)	-	0.36	0.24 (0.15–0.36)	0.17	0.15 (0.13–0.17)
α	-	0.55	0.71 (0.55–0.86)	1.11	0.86 (0.54–1.11)
ω_{0A} (440 nm)	-	0.92	0.87 (0.82–0.92)	0.87	0.84 (0.79–0.87)
ω_{0A} (670 nm)	-	0.92	0.87 (0.81–0.92)	0.88	0.84 (0.79–0.88)
ω_{0A} (870 nm)	-	0.91	0.87 (0.81–0.91)	0.89	0.85 (0.80–0.89)
ω_{0A} (1020 nm)	-	0.91	0.88 (0.84–0.92)	0.91	0.87 (0.84–0.91)
V_{c1}	μm^3 μm^{-2}	0.02	0.01 (0.01–0.02)	0.02	0.01 (0.01–0.02)
V_{c2}	μm^3 μm^{-2}	0.20	0.16 (0.09–0.31)	0.05	0.09 (0.05–0.13)
Effective radius	μm	0.84	1.15 (0.72–1.63)	0.56	1.06 0.56–1.34)

[a]Range shown in parentheses.

[b]Here $\delta_A\lambda$, aerosol optical depth; ω_{0A}, single scattering albedo; α, Angström exponent; V_{c1}, volume concentration of fine mode particles; V_{c2}, volume concentration of coarse mode particles.

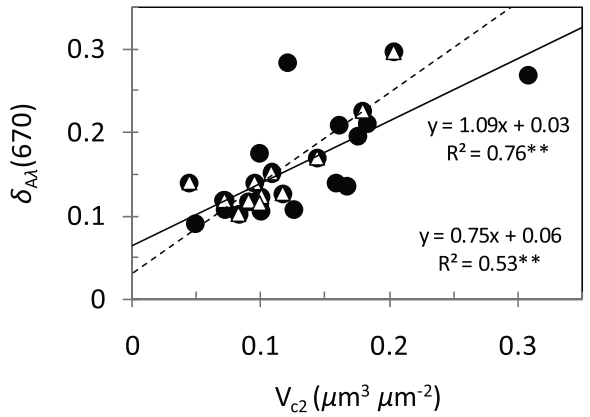

Figure 4. Relationship between aerosol optical depth ($\delta_A\lambda$) at 670 nm and volume concentration of the coarse mode (V_{c2}) (solid circles) and for particulate matter loading higher than 50 mg m^{-2} d^{-1} (open triangles). Regression line equations, R^2 values, and significance (** $p < 0.01$) are shown.

marine air masses. The high Fe content of Saharan-dominated samples would be expected to result in quenching of fluorescence by Fe-DOM complexes [*Ohno et al.*, 2008]. Therefore, the total fluorescence of Saharan-dominated samples (Table 1) is probably even higher. The effects of metal quenching on the fluorescence signatures of organic aerosols merit further study.

[36] The higher molar fluorescence of reduced quinones, particularly the hydroquinone-like component C4, of Saharan-dominated than marine-dominated deposition indicates that the quinone-like compounds that produce fluorescence at these wavelengths are more prevalent in Saharan dust. C4 is a component that appears to be ubiquitous, having been identified in several PARAFAC models [*Cory and McKnight*, 2005; *Stedmon and Markager*, 2005; *Yamashita and Jaffe*, 2008], and associated with microbial reduction of aquatic fulvic acids [*Cory and McKnight*, 2005], as can occur in reducing zones associated with soils and sediments. The large amount of C4 per mole of WSOC in Saharan-dominated deposition further suggests that WSOC deposited by Saharan air masses is derived in part from soils or other terrestrial sources. Oxidized quinone-like components also represent a large portion of the total fluorescence in our samples (approximately 30%), and it has been suggested that such oxygenated quinone-like compounds could be responsible for the color of brown carbon [*Sun et al.*, 2007].

[37] Interestingly, there was high amino acid-like fluorescence (at Ex/Em 240–280/350–370) in EEMs of both Saharan- and marine-dominated deposition that is often attributed to the presence of tyrosine and tryptophan [*Coble*, 1996; *Cory and McKnight*, 2005; *Stedmon and Markager*, 2005]. Also, the molar absorption at 250 and 280 nm of both Saharan- and marine-dominated deposition may be additionally due to the presence of these aromatic amino acids, which absorb most strongly in this range [*Ross*, 1934]. In the atmosphere, these amino acids are extremely important because of their ability to react with ozone and form organic nitrogen compounds that can influence N deposition as well as the atmospheric water cycle and radiative balance [*Zhang and Anastasio*, 2003]. High amino acid-like fluorescence in marine-derived aerosols is consistent with the

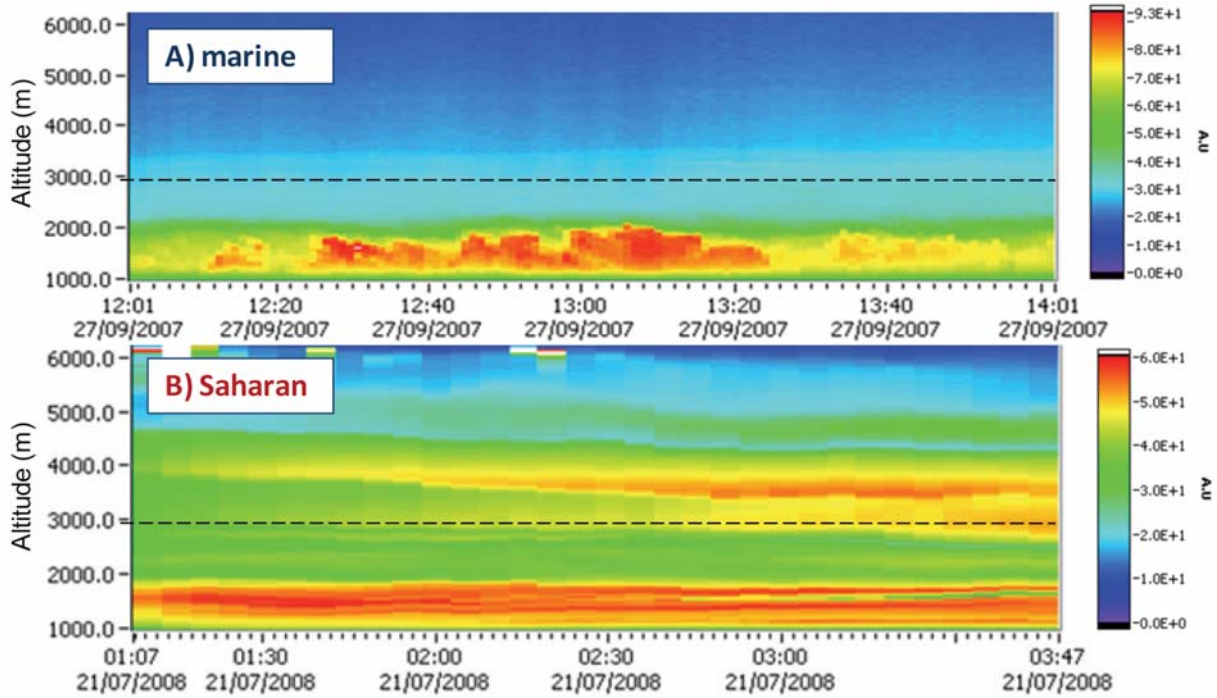

Figure 5. Temporal evolutions of LIDAR signals corresponding to (a) marine-dominated (27 September 2007) and (b) Saharan-dominated (21 July 2008) periods. Legends indicate high (red) to low (violet) absorbance in absorbance units (A.U.). Dashed black line refers to 3000 m asl altitude.

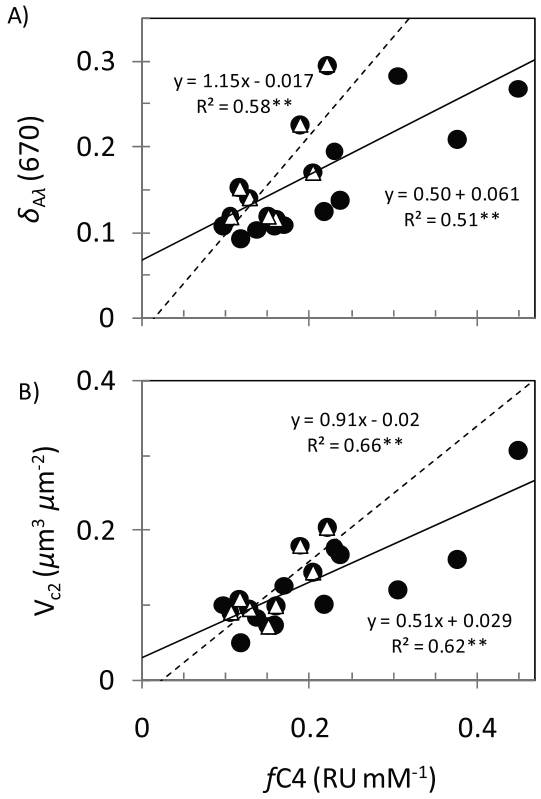

Figure 6. Relationships between molar fluorescence of the hydroquinone-like component (*f*C4, solid circles) and (a) aerosol optical depth at 670 nm ($\delta_A\lambda$) and (b) volume concentration of the coarse mode (V_{c2}). Scatterplots with particulate matter loading higher than 50 mg m^{-2} d^{-1} are also shown (open triangles). Regression line equations, R^2 values, and significance (** $p < 0.01$) are shown.

known injection of amino-nitrogen compounds into the atmosphere through the action of bubble bursting at the sea-air interface [*Milne and Zika*, 1993]. However, until now, little has been reported regarding their presence in high-altitude air masses, such as those reaching the Sierra Nevada at ca. 3000 m asl. Proteinaceous compounds also have been found in cloud water and are associated with the transport of bacteria and viruses, which may promote cloud formation [*Matthias-Maser and Jaenicke*, 1994; *Saxena and Hildemann*, 1995] and act as ice condensation nuclei [*Christner et al.*, 2008]. In the case of Saharan deposition, substantial amounts of humic and fulvic acid-like fluorescent compounds are expected because of the terrestrial sources of dust particles. The explanation for amino acid compounds present in Saharan deposition is less straightforward. If the amino acid compounds, such as tryptophan, result from bacterial products in aerosols as suggested by *Pan et al.* [2009], then the current study supports research showing that microbial material can be transported long distances along with the predominant desert dust load [*Griffin et al.*, 2001, 2007; *Hervàs et al.*, 2009]. Another potential source for this amino acid-like fluorescence in Saharan aerosol deposition may be the release of free amino acid-like compounds from fulvic acids resulting from phototransformations during dust transport [*Tarr et al.*, 2001; *Zhang and Anastasio*, 2003]. This would suggest that UV radiation breaks down the terrestrially derived humic and fulvic-like compounds into lower molecular weight compounds that fluoresce more intensely at lower Ex/Em wavelengths. Then, variations in the amounts of amino acid-like fluorescence may be due, to some extent, to time of transport and aging of HULIS in Saharan aerosols.

[38] Differences were also evident between Saharan and marine-dominated periods for aerosol columnar properties. The mean and range of $\delta_{A\lambda}$ and $\omega_{0A\lambda}$ observed for Saharan-dominated periods were consistent with previous values measured in and near Granada during Saharan dust episodes [*Lyamani et al.*, 2006a; *Alados-Arboledas et al.*, 2008]. Our $\omega_{0A\lambda}$ values are lower than those obtained by other authors for desert dust [*Kaufman et al.*, 2001; *Tanré et al.*, 2001; *Dubovik et al.*, 2002]. These authors obtained values of $\omega_{0A\lambda}$ (670 nm) in the range 0.95–0.99 for situations representative of pure desert dust. This difference is due to the anthropogenic contribution during dust events observed in Granada. *Perrone et al.* [2005] obtained $\omega_{0A\lambda}$ values in the same range that we report here using AERONET measurements made in southern Italy during situations affected by both Saharan dust and central Mediterranean anthropogenic aerosols. Also, *Sokolik and Toon* [1999] have shown that aerosol properties, including single scattering albedo, are very sensitive to the individual minerals and their mixtures and that $\omega_{0A\lambda}$ values increase clearly with wavelength. In contrast, for the Saharan dust dominated periods of this study, the spectral dependence of the single scattering albedo is almost neutral. A similar $\omega_{0A\lambda}$ behavior was measured by ground-based Sun/sky radiometers in the Persian Gulf by *Smirnov et al.* [2002] and in Bahrain by *Dubovik et al.* [2002]. Also similar $\omega_{0A\lambda}$ values were measured in Granada by *Lyamani et al.* [2006a] during a situation affected by Saharan dust and anthropogenic aerosols. The variation in observations is probably due to the mixing of dust with anthropogenic aerosols, the difference in dust compositions, or the difference in dust intensity.

[39] Desert dust particles are larger than other aerosols and, thus, the higher volume concentration of coarse particles (>0.5 μm) compared to fine particles (<0.5 μm) observed here is also consistent with the presence of Saharan dust in the atmosphere [*Lyamani et al.*, 2006b]. This is further supported by the significant positive relationship between $\delta_{A\lambda}$ and V_{c2}, which indicates that the extinction of light increases due to the greater volume of coarse dust particles. This same highly significant relationship was observed by *Alados-Arboledas et al.* [2008] during a Saharan dust episode.

4.2. Urban Influence During Marine-Dominated Periods

[40] For the marine-dominated periods, mean values were higher for $\delta_{A\lambda}$ and lower for $\omega_{0A\lambda}$ than those reported for pure oceanic air masses (see estimates for Lanai, Hawaii, in the work of *Dubovik et al.* [2002]). These values are consistent with those observed in Granada and its vicinity (Armilla) during urban air pollution events [*Alados-Arboledas et al.*, 2008] and when Saharan air masses are not present [*Lyamani et al.*, 2006a, 2006b]. The lower concentration of aerosols during marine periods combined with the often high

concentration of urban aerosols below 2000 m asl, as seen in the LIDAR images, suggest that the marine aerosol influence is not adequately recorded with ground-based remote sensing. In marine air, there are fewer particles to influence the columnar data retrieval and columnar measurements of marine air in an urban setting will be dominated instead by urban aerosols.

4.3. Relationships Between Aerosol Deposition and Columnar Aerosol Properties

[41] The situation just described represents important limitations in comparing relationships between PM deposition at altitude and aerosol properties of the total air column. To overcome this limitation, we also examined relationships for periods that included only PM loading >50 mg m^{-2} d^{-1}. This selection of data showed that, although there were significant initial relationships between WINSOC loading and $\omega_{0A\lambda}$ and between WSOC loading and $\omega_{0A\lambda}$ at all wavelengths, these relationships were not robust enough when the low PM loading periods were removed from the analysis. These results show that the relationships between deposition and $\omega_{0A\lambda}$ are particularly susceptible to the presence of urban aerosols and that caution should be used when comparing deposition data from the high-elevation site with total air column data obtained from a lower-elevation site.

[42] In contrast to relationships with $\omega_{0A\lambda}$, the relationships between molar fluorescence of reduced quinones, in particular *f*C4, and $\delta_{A\lambda}$ at all wavelengths were positive and significant, irrespective of the data set used (high and all PM loadings). Given that an increase in aerosol optical depth is due both to a greater number of particles and light absorption, this result suggests that reduced quinone-like compounds, in particular those associated with terrestrial humic (plant/soil) sources, were probably responsible to some extent for light absorption by bulk aerosols. This may further imply that, in addition to absorption of solar radiation by elemental carbon [*Charlson et al.*, 1992], absorption of solar radiation may be due to reduced quinone-like compounds in organic aerosols. Although iron is undisputedly present in aerosols originating from desert dust [*Jickells et al.*, 2005], there were no significant relationships between total iron concentration and any columnar properties, for all sampling periods as well as for periods with PM loadings >50 mg m^{-2} d^{-1}. Therefore, iron content is not likely to influence the relationships we report between aerosol columnar and optical properties.

[43] The significant relationships between V_{c2} and *f*RQ, and in particular with *f*C4, using both data sets (high and all PM loadings) further suggest that reduced quinone-like compounds may be present in higher amounts in the coarse mode particles. A larger volume of coarse mode particles is typical for dust events [*Dubovik et al.*, 2002], and these results may, therefore, further support the greater contribution of reduced quinone-like compounds to the Saharan aerosol. Also, given that particle size distribution, including volume concentration of coarse mode particles, is a function of sky radiance and aerosol optical depth [*Olmo et al.*, 2008], the significant relationship with reduced quinone-like fluorescence may further reflect the role of reduced quinone-like compounds in light absorption in the atmospheric column.

[44] Finally, the presence of relationships between fluorescent properties of WSOC and columnar properties and the lack of significant relationships between columnar properties and PM and WSOC loadings and UV-vis absorption, underscores the idea that fluorescence provides more specific information on organic aerosol chemical nature than these other properties. Although UV-vis absorption is an important measure of light absorption, the absorption by multiple compounds (e.g., hydroquinone-like and amino acid-like compounds) at the same wavelengths (between 250 and 280 nm) may be a confounding factor in identifying relationships between WSOC absorption and columnar properties. Therefore, the capability of 3-D fluorescence to identify individual fluorescent components poses a real advantage over other measurements of organic matter chemical character and provides an additional layer of information about spectrally active organic compounds, such as amino acid and quinone-like moieties, that may have important applications in atmospheric science.

5. Conclusions and Implications

[45] The results of this study confirm previous findings that WSOC in Saharan-dominated dry deposition contains chromophoric and fluorescent compounds [*Mladenov et al.*, 2008, 2009] that have generally been characterized as humic-like. Moreover, this study highlights that amino acid-like fluorescence is particularly important not only in marine-derived aerosols, but also in Saharan-derived deposition. New relationships found between reduced quinone-like fluorescence and aerosol optical depth are especially important because this last parameter is widely used for characterization of aerosol sources and, in particular, for calculating the aerosol index. If the contribution of quinone-like compounds to aerosols from different sources can be quantified, then atmospheric models can begin to include a higher level of detail in modeling aerosol sources and transformation. The amount of reduced quinone-like compounds in aerosols also has important implications for air pollution studies. Given that reduced quinone compounds in urban air, specifically the redox active species, hydroxyquinones, are associated with asthma and respiratory illness [*Billet et al.*, 2007], the potential for tracking these compounds with fluorescence spectroscopy and with rapid assessments, such as Sun photometry measurements, merits further research.

[46] **Acknowledgments.** The authors gratefully acknowledge the National Oceanic and Atmospheric Administration (NOAA) Air Resources Laboratory (ARL) for use of the Hybrid Single-Particle Lagrangian Integrated Trajectory (HYSPLIT) model and Real-Time Environmental Applications and Display System (READY) website, and the Ministerio de Medio Ambiente and Medio Rural y Marino, the Consejo Superior de Investigaciones Científicas, and the Agencia Estatal de Meteorología of Spain for the use of atmospheric pollution data from the Calima project. We are grateful to the Sierra Nevada National Park Office for providing access and to the staff of the Observatorio de Sierra Nevada (Instituto de Astrofísica de Andalucía, Consejo Superior de Investigaciones Científicas (CSIC), Granada, Spain) for their support with atmospheric deposition samplers. We would like to thank J. López-Ramos, T. Serrano, R. Morales-Baquero, and R. McGrath who helped with sample collection and processing. Funding was provided by Fundación Banco Bilbao Vizcaya–Argentaria (BBVA; BIOCON04/009), Ministerio de Medio Ambiente (080/2007) to I.R., Junta de Andalucía (RNM-01503 and RNM-3568) to L.A.-A. and F.J.O., and Spanish Ministry of Education (CGL2007-66477-C02-01 and CSD2007–00067).

References

Alados-Arboledas, L., H. Lyamani, and F. J. Olmo (2003), Aerosol size properties at Armilla, Granada (Spain), *Q. J. R. Meteorol. Soc.*, *129*(590), 1395–1413, doi:10.1256/qj.01.207.

Alados-Arboledas, L., J. L. Guerrero-Rascado, H. Lyamani, F. Navas-Guzmán, and F. J. Olmo (2007), Characterization of the atmospheric aerosol by combination of LIDAR and sun-photometry, *Proc. SPIE*, *6750*, 67500J–1, doi:10.1117/12.737557.

Alados-Arboledas, L., et al. (2008), Aerosol columnar properties retrieved from CIMEL radiometers during VELETA 2002, *Atmos. Environ.*, *42*(11), 2654–2667, doi:10.1016/j.atmosenv.2007.10.006.

Alcántara, A., F. J. Olmo, and L. Alados-Arboledas (2004), Langley calibrations of sun photometer at Sierra Nevada, Granada, Spain, *Opt. Apl.*, *37*, 3263–3269.

Alfaro, S. C., S. Lafon, J. L. Rajot, P. Formenti, A. Gaudichet, and M. Maille (2004), Iron oxides and light absorption by pure desert dust: An experimental study, *J. Geophys. Res.*, *109*, D08208, doi:10.1029/2003JD004374.

American Public Health Association (APHA) (1992), *Standard Methods for the Examination of Water and Wastewater*, 18th ed., Washington, D. C.

Andreae, M. O., and A. Gelencser (2006), Black carbon or brown carbon? The nature of light-absorbing carbonaceous aerosols, *Atmos. Chem. Phys.*, *6*, 3131–3148.

Billet, S., G. Garçon, Z. Dagher, A. Verdin, F. Ledoux, F. Cazier, D. Courcot, A. Aboukais, and P. Shirali (2007), Ambient particulate matter (PM2.5), Physicochemical characterization and metabolic activation of the organic fraction in human lung epithelial cells (A549), *Environ. Res.*, *105*, 212–223, doi:10.1016/j.envres.2007.03.001.

Charlson, R. J., S. E. Schwartz, J. M. Hales, R. D. Cess, J. A. Coakley Jr., J. E. Hansen, and D. J. Hofmann (1992), Climate forcing by anthropogenic aerosols, *Science*, *255*(5043), 423–430, doi:10.1126/science.255.5043.423.

Chin, Y., G. Aiken, and E. O'Loughlin (1994), Molecular weight, polydispersivity and spectroscopic properties of aquatic humic substances, *Environ. Sci. Technol.*, *28*, 1853–1858, doi:10.1021/es00060a015.

Christner, B. C., C. E. Morris, C. M. Foreman, R. Cai, and D. C. Sands (2008), Ubiquity of biological ice nucleators in snowfall, *Science*, *319*, doi:10.1126/science.1149757.

Coble, P. G. (1996), Characterization of marine and terrestrial DOM in seawater using excitation-emission matrix spectroscopy, *Mar. Chem.*, *51*, 325–346, doi:10.1016/0304-4203(95)00062-3.

Cory, R. M., and D. M. McKnight (2005), Fluorescence spectroscopy reveals ubiquitous presence of oxidized and reduced quinones in dissolved organic matter, *Environ. Sci. Technol.*, *39*, 8142–8149, doi:10.1021/es0506962.

Decesari, S., M. C. Facchini, E. Matta, F. Lettini, M. Mircea, S. Fuzzi, E. Tagliavini, and J. P. Putaud (2001), Chemical features and seasonal variation of fine aerosol water-soluble organic compounds in the Po Valley, Italy, *Atmos. Environ.*, *35*, 3691–3699, doi:10.1016/S1352-2310(00)00509-4.

Draxler, R. R., and G. D. Rolph (2003), HYSPLIT (HYbrid Single-Particle Lagrangian Integrated Trajectory) Model, Air Resour. Lab., Natl. Oceanic and Atmos. Admin., Silver Spring, Md. (Available at http://www.arl.noaa.gov/ready/hysplit4.html)

Duarte, R. M. B. O., C. A. Pio, and A. C. Duarte (2004), Synchronous scan and excitation-emission matrix fluorescence spectroscopy of water-soluble organic compounds in atmospheric aerosols, *J. Atmos. Chem.*, *48*, 157–171, doi:10.1023/B:JOCH.0000036845.82039.8c.

Dubovik, O., B. Holben, T. F. Eck, A. Smirnov, Y. J. Kaufman, M. D. King, D. Tanre, and I. Slutsker (2002), Variability of absorption and optical properties of key aerosol types observed in worldwide locations, *J. Atmos. Sci.*, *59*, 590–608, doi:10.1175/1520-0469(2002)059<0590:VOAAOP>2.0.CO;2.

Griffin, D. W., C. A. Kellogg, and E. A. Shinn (2001), Dust in the wind: Long range transport of dust in the atmosphere and its implications for global public and ecosystem health, *Glob. Change Hum. Health*, *2*, 20–33, doi:10.1023/A:1011910224374.

Griffin, D. W., N. Kubilay, M. Koc-akb, M. A. Gray, T. C. Borden, and E. A. Shinn (2007), Airborne desert dust and aeromicrobiology over the Turkish Mediterranean coastline, *Atmos. Environ.*, *41*, 4050–4062, doi:10.1016/j.atmosenv.2007.01.023.

Guerrero-Rascado, J. L., B. Ruiz, and L. Alados-Arboledas (2008), Multispectral Lidar characterization of the vertical structure of Saharan dust aerosol over southern Spain, *Atmos. Environ.*, *42*, 2668–2681, doi:10.1016/j.atmosenv.2007.12.062.

Hervàs, A., L. Camarero, I. Reche, and E. O. Casamayor (2009), Viability and potential for immigration of airborne bacteria from Africa that reach high mountain lakes in Europe, *Environ. Microbiol.*, *11*, 1612–1623, doi:10.1111/j.1462-2920.2009.01926.x.

Holben, B. N., et al. (1998), Aeronet- a federated instrument network and data archive for aerosol characterization, *Remote Sens. Environ.*, *66*, 1–19, doi:10.1016/S0034-4257(98)00031-5.

Hood, E. D., M. McKnight, and M. W. Williams (2003), Sources and chemical character of dissolved organic carbon across an alpine/subalpine ecotone, Green Lakes Valley, Colorado Front Range, United States, *Water Resour. Res.*, *39*(7), 1188, doi:10.1029/2002WR001738.

Jacobson, M. C., H. C. Hansson, K. J. Noone, and R. J. Charlson (2000), Organic atmospheric aerosols: Review and state of the science, *Rev. Geophys.*, *38*, 267–294, doi:10.1029/1998RG000045.

Jaffrezo, J. L., G. Aymoz, C. Delaval, and J. Cozic (2005), Seasonal variations of the water soluble organic carbon mass fraction of aerosol in two valleys of the French Alps, *Atmos. Chem. Phys.*, *5*, 2809–2821.

Jickells, T. D., et al. (2005), Global iron connections between desert dust, ocean biogeochemistry, and climate, *Science*, *308*, 67–71, doi:10.1126/science.1105959.

Kaufman, Y. J., D. Tanré, O. Dubovik, A. Karnieli, and L. A. Remer (2001), Absorption of sunlight by dust as inferred from satellite and ground-based remote sensing, *Geophys. Res. Lett.*, *28*(8), 1479–1482, doi:10.1029/2000GL012647.

Kieber, R. J., R. F. Whitehead, S. N. Reid, J. D. Willey, and P. J. Seaton (2006), Chromophoric dissolved organic matter (CDOM) in rainwater, southeastern North Carolina, USA, *J. Atmos. Chem.*, *54*, 21–41, doi:10.1007/s10874-005-9008-4.

Kieber, R. J., J. D. Willey, R. F. Whitehead, and S. N. Reid (2007), Photobleaching of chromophoric dissolved organic matter (CDOM) in rainwater, *J. Atmos. Chem.*, *58*, 219–235, doi:10.1007/s10874-007-9089-3.

Krivácsy, Z., et al. (2001), Study on the chemical character of water soluble organic compounds in fine atmospheric aerosol at the Jungfraujoch, *J. Atmos. Chem.*, *39*, 235–259, doi:10.1023/A:1010637003083.

Laurion, I., M. Ventura, J. Catalan, R. Psenner, and R. Sommaruga (2000), Attenuation of ultraviolet radiation in mountain lakes: Factors controlling the among- and within-lake variability, *Limnol. Oceanogr.*, *45*, 1274–1288.

Linke, C., O. Mohler, A. Veres, Á. Mohácsi, Z. Bozóki, G. Szabó, and M. Schnaiter (2006), Optical properties and mineralogical composition of different Saharan mineral dust samples: A laboratory study, *Atmos. Chem. Phys.*, *6*, 3315–3323.

Lyamani, H., F. J. Olmo, and L. Alados-Arboledas (2005), Saharan dust outbreak over south-eastern Spain as detected by Sun photometer, *Atmos. Environ.*, *39*, 7276–7284.

Lyamani, H., F. J. Olmo, A. Alcántara, and L. Alados-Arboledas (2006a), Atmospheric aerosols during the 2003 heat wave in southeastern Spain II: Microphysical columnar properties and radiative forcing, *Atmos. Environ.*, *40*, 6465–6476, doi:10.1016/j.atmosenv.2006.04.047.

Lyamani, H., F. J. Olmo, A. Alcántara, and L. Alados-Arboledas (2006b), Atmospheric aerosols during the 2003 heat wave in southeastern Spain I: Spectral optical depth, *Atmos. Environ.*, *40*, 6453–6464, doi:10.1016/j.atmosenv.2006.04.048.

Matthias-Maser, S., and R. Jaenicke (1994), Examination of atmospheric bioaerosol particles with radii >0.2 μm, *J. Aerosol Sci.*, *25*(8), 1605–1613, doi:10.1016/0021-8502(94)90228-3.

McKnight, D. M., E. W. Boyer, P. K. Westerhoff, P. T. Doran, T. Kulbe, and D. T. Andersen (2001), Spectrofluorometric characterization of dissolved organic matter for indication of precursor organic material and aromaticity, *Limnol. Oceanogr.*, *46*, 38–48.

Milne, P. J., and R. G. Zika (1993), Amino acid nitrogen in atmospheric aerosols: Occurrence, sources and photochemical modification, *J. Atmos. Chem.*, *16*, 361–398, doi:10.1007/BF01032631.

Mladenov, N., D. M. McKnight, P. Wolski, and L. Ramberg (2005), Effects of the annual flood on dissolved organic carbon dynamics in the Okavango Delta, Botswana, *Wetlands*, *25*(3), 622–638, doi:10.1672/0277-5212(2005)025[0622:EOAFOD]2.0.CO;2.

Mladenov, N., D. M. McKnight, S. A. Macko, M. Norris, R. M. Cory, and L. Ramberg (2007), Chemical characterization of DOM in channels of a seasonal wetland, *Aquat. Sci.*, *69*(4), 456–471, doi:10.1007/s00027-007-0905-2.

Mladenov, N., E. Pulido-Villena, R. Morales-Baquero, E. Ortega-Retuerta, R. Sommaruga, and I. Reche (2008), Spatio-temporal drivers of dissolved organic matter in high alpine lakes: The role of Saharan dust inputs and bacterial activity, *J. Geophys. Res.*, *113*, G00D01, doi:10.1029/2008JG000699.

Mladenov, N., J. López-Ramos, D. M. McKnight, and I. Reche (2009a), Alpine lake optical properties as sentinels of dust deposition and global change, *Limnol. Oceanogr.*, *54*, 2386–2400.

Mladenov, N., Y. Zheng, M. P. Miller, D. Nemergut, T. Legg, B. Simone, C. Hageman, M. Rahman, K. Ahmed, and D. M. McKnight (2009b), Dissolved organic matter sources and consequences for iron and arsenic mobilization in Bangladesh, *Environ. Sci. Technol.*, doi:10.1021/es901472g.

Morales-Baquero, R., E. Pulido-Villena, and I. Reche (2006), Atmospheric inputs of phosphorus and nitrogen to the southwest Mediterranean region: Biogeochemical responses of high mountain lakes, *Limnol. Oceanogr.*, *51*, 830–837.

Morris, D. P., H. Zagarese, C. E. Williamson, E. G. Balseiro, B. R. Hargreaves, B. Modenutti, R. Moeller, and C. Queimalinos (1995), The attenuation of solar UV radiation in lakes and the role of dissolved organic carbon, *Limnol. Oceanogr.*, *40*, 1381–1391.

Muller, C., A. Baker, R. Hutchinson, I. J. Fairchild, and C. Kidd (2008), Analysis of rainwater dissolved organic carbon compounds using fluorescence spectrophotometry, *Atmos. Environ.*, *42*, 8036–8045, doi:10.1016/j.atmosenv.2008.06.042.

Nakajima, T., G. Tonna, R. Rao, P. Boi, Y. J. Kaufamn, and B. N. Holben (1996), Use of the brightness measurements from ground for remote sensing of particulate polydispersions, *Appl. Opt.*, *35*, 2672–2686, doi:10.1364/AO.35.002672.

Ohno, T., A. Amirbahman, and R. Bro (2008), Parallel factor analysis of excitation–emission matrix fluorescence spectra of water soluble soil organic matter as basis for the determination of conditional metal binding parameters, *Environ. Sci. Technol.*, *42*, 186–192.

Olmo, F. J., A. Quirantes, A. Alcántara, H. Lyamani, and L. Alados-Arboledas (2006), Preliminary results of a non-spherical aerosol method for the retrieval of the atmospheric aerosol optical properties, *J. Quant. Spectrosc. Radiat. Transfer*, *100*, 305–314, doi:10.1016/j.jqsrt.2005.11.047.

Olmo, F. J., A. Quirantes, V. Lara, H. Lyamani, and L. Alados-Arboledas (2008), Aerosol optical properties assessed by an inversion method using the solar principal plane for non-spherical particles, *J. Quant. Spectrosc. Radiat. Transfer*, *109*, 1504–1516, doi:10.1016/j.jqsrt.2007.12.019.

Pan, Y., R. G. Pinnick, S. C. Hill, and R. K. Chang (2009), Particle-fluorescence spectrometer for real-time single-particle measurements of atmospheric organic carbon and biological aerosol, *Environ. Sci. Technol.*, *43*(2), 429–434, doi:10.1021/es801544y.

Perrone, M. R., M. Santese, A. M. Tafuro, B. N. Holben, and A. Smirnov (2005), Aerosol load characterization over southeast Italy for one year of AERONET Sun photometer measurements, *Atmos. Res.*, *75*(1–2), 111–133, doi:10.1016/j.atmosres.2004.12.003.

Prospero, J. M., and P. J. Lamb (2003), African droughts and dust transport to the Caribbean: Climate change implications, *Science*, *302*, 1024–1027, doi:10.1126/science.1089915.

Pulido-Villena, E., I. Reche, and R. Morales-Baquero (2006), Significance of atmospheric inputs of calcium over the southwestern Mediterranean region: High mountain lakes as tools for detection, *Global Biogeochem. Cycles*, *20*, GB2012, doi:10.1029/2005GB002662.

Reche, I., E. Ortega-Retuerta, O. Romera, E. Pulido-Villena, R. Morales-Baquero, and E. O. Casamayor (2009), Effect of Saharan dust inputs on bacterial activity and community composition in Mediterranean lakes and reservoirs, *Limnol. Oceanogr.*, *54*, 869–879.

Ross, W. F. (1934), The spectroscopic identification of phenylalanine in protein material, *J. Biol. Chem.*, *104*, 531–535.

Saxena, P., and L. M. Hildemann (1995), Water-soluble organics in atmospheric particles: A critical review of the literature and application of thermodynamics to identify candidate compounds, *J. Atmos. Chem.*, *24*, 57–109, doi:10.1007/BF00053823.

Smirnov, A., B. N. Holben, T. F. Eck, O. Dubovik, and I. Slutsker (2000), Cloud-screening and quality control algorithms for the AERONET database, *Remote Sens. Environ.*, *73*(3), 337–349, doi:10.1016/S0034-4257(00)00109-7.

Smirnov, A., B. N. Holben, O. Dubovik, N. T. O'Neill, T. F. Eck, D. L. Westphal, A. K. Goroch, C. Pietras, and L. Slutsker (2002), Atmospheric aerosol optical properties in the Persian Gulf, *J. Atmos. Sci.*, *59*, 620–634, doi:10.1175/1520-0469(2002)059<0620:AAOPIT>2.0.CO;2.

Sokolik, I. N., and O. B. Toon (1999), Incorporation of mineralogical composition into models of the radiative properties of mineral aerosol from UV to IR wavelength, *J. Geophys. Res.*, *104*, 9423–9444, doi:10.1029/1998JD200048.

Stedmon, C. A., and S. Markager (2005), Resolving the variability in dissolved organic matter fluorescence in a temperate estuary and its catchment using PARAFAC analysis, *Limnol. Oceanogr.*, *50*(2), 686–697.

Stedmon, C. A., S. Markager, and R. Bro (2003), Tracing dissolved organic matter in aquatic environments using a new approach to fluorescence spectroscopy, *Mar. Chem.*, *82*, 239–254, doi:10.1016/S0304-4203(03)00072-0.

Steiner, M., and N. Lazaroff (1974), Direct method for continuous determination of iron oxidation by autotrophic bacteria, *Appl. Microbiol.*, *28*(5), 872–880.

Sulzberger, B., and H. Laubscher (1995), Reactivity of various types of iron (II1) (hydr)oxides towards light-induced dissolution, *Mar. Chem.*, *50*, 103–115, doi:10.1016/0304-4203(95)00030-U.

Sun, H., L. Biedermann, and T. C. Bond (2007), The color of brown carbon: A model for ultraviolet and visible light absorption by organic carbon aerosol, *Geophys. Res. Lett.*, *34*, L17813, doi:10.1029/2007GL029797.

Tanré, D., Y. J. Kaufman, B. N. Holben, B. Chatenet, A. Karnieli, F. Lavenu, L. Blarel, O. Dubovik, L. A. Remer, and A. Smirnov (2001), Climatology of dust aerosol size distribution and optical properties derived from remotely sensed data in the solar spectrum, *J. Geophys. Res.*, *106*, 18,205–18,217, doi:10.1029/2000JD900663.

Tarr, M. A., W. W. Wang, T. S. Bianchi, and E. Engelhaupt (2001), Mechanisms of ammonia and amino acid photoproduction from aquatic humic and colloidal matter, *Water Res.*, *35*(15), 3688–3696, doi:10.1016/S0043-1354(01)00101-4.

Velapoldi, R. A., and K. D. Mielenz (1981), A fluorescence standard reference material - quinine sulfate dihydrate, *Appl. Opt.*, *9*, 1718.

Weishaar, J. L., G. R. Aiken, B. A. Bergamaschi, M. S. Fram, R. Fujii, and K. Mopper (2003), Evaluation of specific ultraviolet absorbance as an indicator of the chemical composition and reactivity of dissolved organic carbon, *Environ. Sci. Technol.*, *37*, 4702–4708, doi:10.1021/es030360x.

Yamashita, Y., and R. Jaffe (2008), Characterizing the interactions between trace metals and dissolved organic matter using excitation-emission matrix and parallel factor analysis, *Environ. Sci. Technol.*, *42*, 7374–7379, doi:10.1021/es801357h.

Zhang, Q., and C. Anastasio (2003), Free and combined amino compounds in atmospheric fine particles (PM2.5) and fog waters from Northern California, *Atmos. Environ.*, *37*, 2247–2258, doi:10.1016/S1352-2310(03)00127-4.

L. Alados-Arboledas, H. Lyamani, and F. J. Olmo, Departamento de Física Aplicada, Universidad de Granada, E-18071 Granada, Spain.

N. Mladenov, Institute of Arctic and Alpine Research, University of Colorado at Boulder, Boulder, CO 80305, USA. (mladenov@colorado.edu)

I. Reche, Departamento de Ecología, Universidad de Granada, E-18071 Granada, Spain.